# Solution and refinement of the crystal structure of $Bi_7Ta_3O_{18}$

Christopher D. Ling,[a]* Siegbert Schmid,[a] Ray L. Withers,[a] John G. Thompson,[a] Nobuo Ishizawa[b] and Shunji Kishimoto[c]

[a]*Research School of Chemistry, Australian National University, Canberra, ACT 0200, Australia,* [b]*Materials and Structures Laboratory, Tokyo Institute of Technology, Nagatsuta, Midori-ku, Yokohama 226, Japan, and* [c]*National Laboratory for High Energy Physics, Oho, Tsukuba 305, Japan. E-mail: email: ling@rsc.anu.edu.au*

## Abstract

The structure of heptabismuth tritantalum octadeca-oxide, $Bi_7Ta_3O_{18}$, has been solved and refined using single-crystal X-ray diffraction data collected at a synchrotron source in conjunction with unit-cell and symmetry information derived from electron diffraction. The space-group symmetry is triclinic $C1$ but is very close to monoclinic $C2/m$. A twin component observed during data collection was successfully modelled in the refinement. The $C2/m$ prototype fitted all the Rietveld-refinable features of a medium-resolution neutron powder diffraction pattern. The metal-atom array is approximately face-centred cubic (fluorite type), punctuated by regularly spaced displacement faults perpendicular to the $[111]_{\text{fluorite}}$ direction every 2.5 fluorite unit cells. The metal-atom populations and O-atom positions are fully ordered. The $Ta^{5+}$ cations are octahedrally coordinated, with $TaO_6$ octahedra forming columns. The remaining O atoms occupy distorted fluorite positions. The $Bi^{3+}$ cations occupy octahedral, square pyramidal or trigonal prismatic sites within the O-atom array; strain in the latter coordination environment appears to be responsible for the lowering of symmetry from mono-clinic to triclinic.

## 1. Introduction

The high-temperature form of bismuth oxide, $\delta$-$Bi_2O_3$, is one of the best oxygen-ion conductors known (Taka-hashi & Iwahara, 1978; Sleight, 1980). It is reported as a face-centred-cubic (f.c.c.) fluorite-type structure, with 25% average oxygen vacancies accounting for its anionic conduction properties (Gattow & Schröder, 1962; Harwig, 1978). The fact that $\delta$-$Bi_2O_3$ cannot be quen-ched to room temperature has created interest in bismuth-rich phases in binary oxide systems involving certain transition metal oxides. Phases in many of these systems appear to form modulated structures preserving both the underlying fluorite-related substructure and the ionic conduction properties of $\delta$-$Bi_2O_3$ (Allnat & Jacobs, 1961, 1967).

One such system is the $Bi_2O_3$–$Ta_2O_5$ system, investi-gated in an X-ray powder diffraction (XRD) study by Levin & Roth (1964) and more recently in a transmis-sion electron microscopy (TEM) study by Zhou (1992). Zhou reported the new phase $Bi_7Ta_3O_{18}$ as a 'type II*' commensurately modulated $\delta$-$Bi_2O_3$-related (super-structure) phase.

In our recent reinvestigation of bismuth-rich phases in a number of binary oxide systems (Ling *et al.*, 1998), we reproduced the electron diffraction patterns reported for $Bi_7Ta_3O_{18}$, but derived a unit cell apparently unre-lated to that reported by Zhou. There was no unam-biguous fluorite-type subcell underlying this unit cell, despite observation of a number of ostensibly fluorite-like projections of the reciprocal sublattice. Synchrotron XRD data also showed a pseudo-fluorite-type reciprocal lattice which could not be unambiguously indexed as fluorite. It was concluded that while $Bi_7Ta_3O_{18}$ might contain structural elements of $\delta$-$Bi_2O_3$, it must be too far removed from that prototype to be usefully described as a modulated variant thereof.

We have now synthesized $Bi_7Ta_3O_{18}$ as a single-phase powder in sufficient quantities for the collection of neutron powder diffraction data. The greater relative contribution of O atoms to neutron scattering compared with their contribution to X-ray scattering provides an independent check on refined O-atom parameters. Crystals of sufficient size for the collection of X-ray diffraction data at a synchrotron source have also been grown. Here we report and discuss the structure of $Bi_7Ta_3O_{18}$.

## 2. Experimental

### 2.1. Single-crystal X-ray diffraction

Crystals of $Bi_7Ta_3O_{18}$ were grown by solid-state reaction of a mixture of $Bi_2O_3$ (Koch–Lite, 99.998%) and $Ta_2O_5$ (Aldrich, 99.99%) in a molar ratio of 17:8. The mixture was heated in a platinum crucible to 1473 K then cooled to 1123 K over 160 h before quenching to room temperature. Small transparent yellow plate-like crystals were formed on the surface of the specimen.

Single-crystal X-ray diffraction data were collected at the Photon Factory (KEK, Tsukuba, Japan) in order that the smallest possible crystals could be used, minimizing

Table 1. *Details of the single-crystal X-ray diffraction experiment*

| Crystal data | |
|---|---|
| Chemical formula | Bi$_7$Ta$_3$O$_{18}$ |
| Chemical formula weight | 2293.71 |
| Cell setting | Triclinic |
| Space group | $C1$ |
| $a$ (Å) | 34.005 (3) |
| $b$ (Å) | 7.6024 (4) |
| $c$ (Å) | 6.6358 (5) |
| $\alpha$ (°) | 90.086 (6) |
| $\beta$ (°) | 109.127 (6) |
| $\gamma$ (°) | 90.043 (6) |
| $V$ (Å$^3$) | 1620.8 (2) |
| $Z$ | 4 |
| $D_x$ (Mg m$^{-3}$) | 9.4 |
| Radiation type | Synchrotron X-ray |
| Wavelength (Å) | 0.9580 (4) |
| No. of reflections for cell parameters | 25 |
| $\theta$ range (°) | 22.76–37.98 |
| $\mu$ (mm$^{-1}$) | 85.4 |
| Temperature (K) | 293 |
| Crystal form | Plate |
| Crystal size (mm) | 0.020 × 0.020 × 0.002 |
| Crystal colour | Yellow |
| | |
| Data collection | |
| Diffractometer | Tsukuba |
| Data collection method | $\omega$ scans |
| Absorption correction | Gaussian |
| $T_{\min}$ | 0.277 |
| $T_{\max}$ | 0.844 |
| No. of measured reflections | 17 604 |
| No. of independent reflections | 13 798 |
| No. of observed reflections | 11 796 |
| Criterion for observed reflections | $F^2 > 3\sigma(F^2)$ |
| $R_{\text{int}}$ | 0.023 |
| $\theta_{\max}$ (°) | 50 |
| Range of $h, k, l$ | $-54 \rightarrow h \rightarrow 54$ |
| | $-12 \rightarrow k \rightarrow 12$ |
| | $-10 \rightarrow l \rightarrow 10$ |
| No. of standard reflections | 6 |
| Frequency of standard reflections | Every 200 reflections |
| Intensity decay (%) | 0 |
| | |
| Refinement | |
| Refinement on | $F^2$ |
| $R[F^2 > 2\sigma(F^2)]$ | 0.0386 |
| $wR(F^2)$ | 0.0337 |
| $S$ | 1.2490 |
| No. of reflections used in refinement | 11 796 |
| No. of parameters used | 327 |
| Weighting scheme | $w = 1/\sigma^2(F)$ |
| $(\Delta/\sigma)_{\max}$ | 0.00118 |
| $\Delta\rho_{\max}$ (e Å$^{-3}$) | 5.80 |
| $\Delta\rho_{\min}$ (e Å$^{-3}$) | $-5.61$ |
| Extinction method | Zachariasen (1968) |
| Extinction coefficient | 1828 (30) |
| Source of atomic scattering factors | *International Tables for X-ray Crystallography* (1974, Vol. IV, Tables 2.2B and 2.3.1) |

absorption and reducing the probability of twinning. Experimental details for the diffraction experiment are summarized in Table 1. *Xtal*3.2 (Hall *et al.*, 1992) was used for all calculations.

Electron diffraction and XRD indicated that the symmetry was probably monoclinic $C2/m$ (Ling *et al.*, 1998). Strong twinning was observed against the monoclinic *b* axis in this setting, and some difficulty was experienced in finding an untwinned crystal. Very small plates ($\sim$20 µm across and 1–2 µm thick) were found to be relatively twin-free. When ostensibly untwinned crystals were found, however, it was noted that the angles $\alpha$ and $\gamma$, constrained to 90° in $C2/m$, in fact reproducibly deviated from 90° by approximately 0.08 and 0.05°, respectively. Furthermore, peak splitting was observed in high-angle $\omega$ scans (principally along the *b* axis) corresponding to twinning against these slightly non-90° angles. On this basis it was concluded that the symmetry was in fact triclinic ($C\bar{1}$ or $C1$). Although this twinning was never eliminated, the major twin component of the crystal ultimately chosen for data collection contributed approximately 95% of the total intensity. Because the majority of peaks were not split sufficiently for separate data collection, data were collected using 1°-wide $\omega$ scans in order that the full intensity from both components would be collected for all reflections.

An absorption correction was applied with the crystal approximated to a circular plate 20 µm in diameter and 2 µm thick (normal to the long axis *a*).

### 2.2. Powder neutron diffraction

A powder sample of Bi$_7$Ta$_3$O$_{18}$ was prepared by solid-state reaction of a mixture of Bi$_2$O$_3$ (Koch–Lite, 99.998%) and Ta$_2$O$_5$ (Aldrich, 99.99%) in a molar ratio of 7:3 in a platinum crucible at 1173 K for 0.5 h. The sample was quenched to room temperature, reground, annealed in a sealed platinum vessel at 1173 K for 168 h and again quenched to room temperature. A homogeneous pale-yellow powder was obtained and identified as single-phase Bi$_7$Ta$_3$O$_{18}$ by XRD (Jungner XDC-700 Guinier–Hägg camera) (Ling *et al.*, 1998).

Powder neutron diffraction data were collected on POLARIS (Hull *et al.*, 1992), the high-flux medium-resolution instrument at ISIS (Rutherford Appleton Laboratories, UK). We sought the high-flux instrument POLARIS in order to use a small sample; we had experienced difficulties obtaining a large, homogenous sample *via* the method described above. Experimental details for the diffraction experiment are summarized in Table 2. The resolution was not sufficient to observe the small triclinic splitting described in §2.1.

### 3. Refinement

An initial model for the structure of the metal-atom array was obtained using direct methods on the single-crystal data set in the high symmetry $C2/m$ setting. Occupational and positional parameters were refined,

**Table 2.** *Details of the powder neutron diffraction experiment*

Crystal data

| | |
|---|---|
| Chemical formula | $Bi_7Ta_3O_{18}$ |
| Chemical formula weight | 2293.71 |
| Cell setting | Monoclinic |
| Space group | $C2/m$ |
| $a$ (Å) | 34.0084 (9) |
| $b$ (Å) | 7.60686 (20) |
| $c$ (Å) | 6.63644 (17) |
| $\beta$ (°) | 109.2375 (11) |
| $V$ (Å³) | 1620.94 (7) |
| $Z$ | 4 |
| Temperature (K) | 293 |
| Radiation type | Neutron |
| Specimen shape | Cylinder |
| Specimen size (mm) | $25 \times 8 \times 8$ |
| Preparation conditions | Sealed Pt tube, 101.3 kPa, 1173 K |
| Particle morphology | Plate |
| Colour | Yellow |

Data collection

| | |
|---|---|
| Instrument | POLARIS |
| Detectors | $^3$He gas and ZnS scintillation counters |
| Data collection method | Time-of-flight scans |
| Specimen mounting | Vanadium can |

| | |
|---|---|
| $R_p$ | 0.0455 |
| $R_{wp}$ | 0.0342 |
| $S$ | 5.41 |
| Profile function | Exponential pseudo-Voigt convolution (Von Dreele, 1990) |
| No. of parameters | 116 |
| Source of atomic scattering factors | *International Tables for Crystallography* (1992, Vol. C) |

**Table 3.** *Comparative refinement statistics for the single-crystal X-ray refinement of $Bi_7Ta_3O_{18}$*

All atoms were refined with isotropic displacement parameters.

| Space group | $R$ | $wR$ | $S$ |
|---|---|---|---|
| $C2/m$ | 0.1951 | 0.1791 | 5.1254 |
| $C\bar{1}$ | 0.1776 | 0.1639 | 4.7027 |
| $C2$ | 0.1749 | 0.1634 | 4.8541 |
| $Cm$ | 0.1473 | 0.1416 | 4.4260 |
| $C1$ | 0.0474 | 0.0410 | 1.4968 |
| $C1$ ($Cm$ twin) | 0.0447 | 0.0384 | 1.4301 |

and the metal-atom populations appeared to be fully ordered. On using difference Fourier syntheses to determine the O-atom positions it became clear that many peaks in the difference map were at plausible distances from metal atoms, but implausibly close to each other. It was possible to choose and refine a complete set of plausible O-atom sites, yet the refinement statistics remained poor ($R = 0.195$) and the difference Fourier map retained many extraneous (plausible O-atom) peaks.

This $C2/m$ model was subsequently tested against the powder neutron diffraction profile by the Rietveld method using *GSAS* (Larson & Von Dreele, 1991), in order to corroborate the refined O-atom positions. It was possible to refine all positional and isotropic displacement parameters without any significant atomic shifts developing. The difference between the observed and calculated patterns at this point (Fig. 1) appeared sufficiently small that meaningful refinement of further
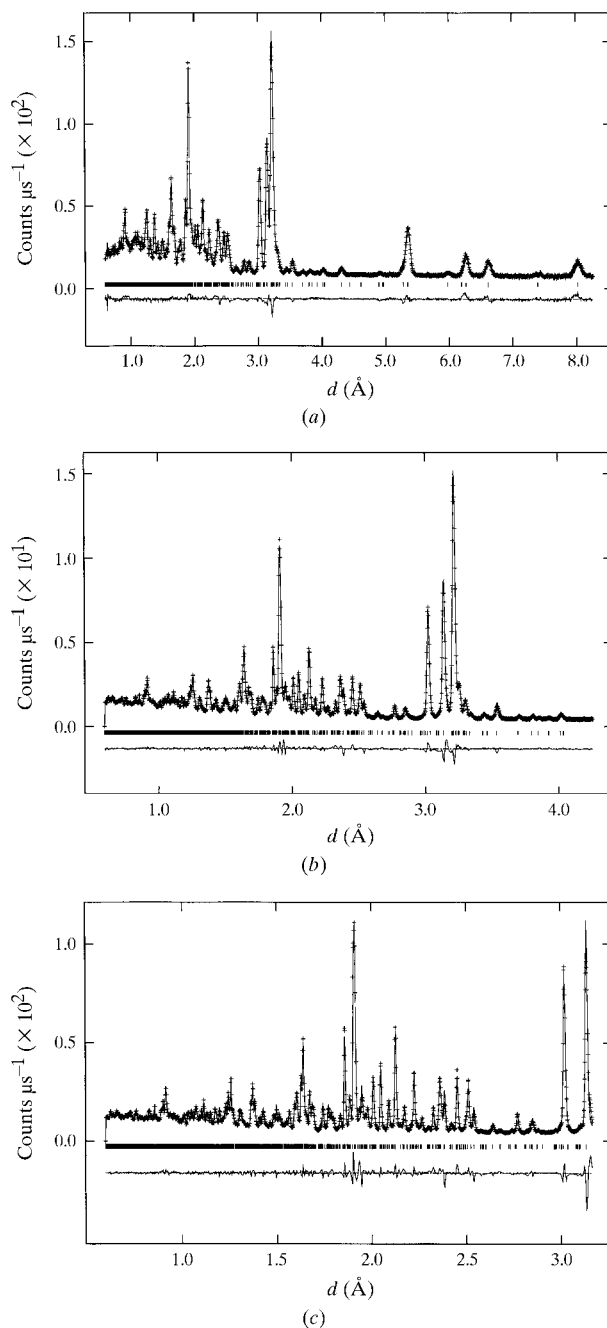


Fig. 1. Observed (crosses), calculated (solid line) and difference (below) neutron powder diffraction profiles for $Bi_7Ta_3O_{18}$ at (*a*) the 35, (*b*) the 90 and (*c*) the 145° detector banks (Hull *et al.*, 1992).

Table 4. *Fractional atomic coordinates and equivalent isotropic displacement parameters ($\mathring{A}^2$) for the single-crystal X-ray (C1) structure*

$$U_{\mathrm{eq}} = (1/3)\Sigma_i\Sigma_j U^{ij}a^i a^j \mathbf{a}_i.\mathbf{a}_j.$$

| | $x$ | $y$ | $z$ | $U_{\mathrm{eq}}$ |
|---|---|---|---|---|
| Bi1 | 0.34035 (3) | 0.23954 (9) | 0.48808 (13) | 0.0175 (4) |
| Bi2 | 0.338481 (19) | −0.49941 (8) | −0.03295 (9) | 0.0077 (3) |
| Bi3 | 0.352745 (18) | 0.00191 (8) | 0.00818 (8) | 0.0078 (3) |
| Ta4 | 0.439500 (19) | 0.25362 (8) | −0.02517 (10) | 0.0053 (2) |
| Bi5 | 0.13920 (2) | 0.25045 (8) | 0.42381 (9) | 0.0084 (3) |
| Ta6 | 0.44073 (2) | −0.24841 (8) | −0.01788 (10) | 0.0052 (3) |
| Bi7 | 0.145987 (18) | −0.49905 (7) | −0.03491 (8) | 0.0074 (3) |
| Ta8 | 0.25045 (2) | −0.25148 (9) | 0.00335 (10) | 0.0055 (2) |
| Bi9 | 0.13846 (2) | −0.25211 (8) | 0.42799 (10) | 0.0106 (3) |
| Bi10 | 0.35341 (2) | −0.25195 (9) | −0.49329 (11) | 0.0149 (4) |
| Bi11 | 0.44582 (2) | 0.01013 (9) | −0.47120 (9) | 0.0108 (3) |
| Ta12 | 0.051995 (18) | −0.25142 (7) | −0.03194 (9) | 0.0052 (3) |
| Bi13 | 0.249612 (19) | −0.00439 (8) | −0.47642 (9) | 0.0076 (3) |
| Bi14 | 0.05081 (2) | 0.00216 (9) | −0.50979 (10) | 0.0095 (3) |
| Ta15 | 0.24956 (2) | 0.25148 (9) | −0.00335 (11) | 0.0059 (2) |
| Bi16 | 0.246719 (19) | −0.49654 (9) | 0.46346 (9) | 0.0090 (3) |
| Bi17 | 0.045577 (19) | −0.49984 (8) | 0.42758 (9) | 0.0097 (3) |
| Ta18 | 0.052326 (18) | 0.25109 (7) | −0.03323 (9) | 0.0049 (3) |
| Bi19 | 0.158172 (19) | −0.00140 (8) | −0.00700 (8) | 0.0088 (3) |
| Bi20 | 0.44170 (2) | −0.50124 (8) | 0.46484 (9) | 0.0079 (3) |
| O1 | 0.4279 (3) | 0.0028 (12) | −0.1082 (13) | 0.0066 (14) |
| O2 | 0.3787 (3) | −0.2898 (13) | −0.1112 (15) | 0.0104 (16) |
| O3 | 0.1165 (3) | −0.2130 (12) | 0.0673 (14) | 0.0084 (15) |
| O4 | 0.3789 (3) | 0.2971 (13) | −0.1083 (15) | 0.0117 (17) |
| O5 | 0.1162 (3) | 0.2103 (11) | 0.0686 (13) | 0.0053 (14) |
| O6 | 0.0674 (3) | 0.2152 (12) | 0.2988 (14) | 0.0068 (15) |
| O7 | 0.4455 (3) | 0.2042 (13) | 0.2681 (15) | 0.0127 (17) |
| O8 | 0.4476 (3) | −0.1953 (13) | 0.2686 (16) | 0.0137 (18) |
| O9 | 0.4247 (3) | −0.2881 (12) | −0.3500 (14) | 0.0096 (16) |
| O10 | 0.4971 (3) | −0.2166 (12) | −0.0312 (14) | 0.0087 (15) |
| O11 | 0.2356 (3) | 0.0006 (13) | −0.0646 (15) | 0.0124 (16) |
| O12 | 0.3814 (3) | −0.0066 (13) | 0.4020 (14) | 0.0095 (15) |
| O13 | 0.2581 (3) | −0.2062 (13) | 0.3109 (15) | 0.0129 (17) |
| O14 | 0.4506 (3) | −0.4968 (13) | 0.0500 (15) | 0.0119 (17) |
| O15 | 0.2662 (3) | 0.2029 (11) | 0.3241 (13) | 0.0085 (14) |
| O16 | 0.1632 (3) | −0.4978 (13) | 0.3090 (14) | 0.0100 (15) |
| O17 | 0.3246 (3) | 0.0028 (14) | −0.3502 (15) | 0.0146 (17) |
| O18 | 0.0456 (3) | −0.0030 (13) | −0.1058 (14) | 0.0110 (16) |
| O19 | 0.3779 (3) | −0.4902 (14) | 0.3089 (15) | 0.0144 (17) |
| O20 | 0.1917 (3) | 0.2938 (12) | −0.0200 (14) | 0.0117 (16) |
| O21 | 0.1131 (3) | 0.0024 (14) | −0.3657 (15) | 0.0144 (17) |
| O22 | 0.1907 (3) | −0.2977 (14) | −0.0463 (16) | 0.0158 (18) |
| O23 | 0.0671 (3) | −0.5002 (13) | 0.0475 (13) | 0.0083 (15) |
| O24 | 0.1805 (3) | 0.0085 (14) | 0.3466 (16) | 0.0142 (18) |
| O25 | 0.1098 (3) | −0.4942 (14) | −0.4592 (16) | 0.0136 (17) |
| O26 | 0.0476 (3) | 0.2990 (12) | −0.3211 (14) | 0.0094 (16) |
| O27 | 0.0687 (3) | −0.2092 (13) | 0.2996 (15) | 0.0106 (16) |
| O28 | 0.2646 (3) | −0.4973 (12) | 0.0867 (14) | 0.0105 (15) |
| O29 | 0.4278 (3) | 0.2940 (13) | −0.3478 (15) | 0.0107 (16) |
| O30 | 0.0448 (3) | −0.2963 (14) | −0.3225 (16) | 0.0148 (18) |
| O31 | 0.3110 (3) | 0.2065 (13) | 0.0623 (15) | 0.0151 (18) |
| O32 | 0.3111 (3) | −0.1971 (14) | 0.0691 (17) | 0.019 (2) |
| O33 | 0.2428 (3) | 0.3012 (15) | −0.2909 (17) | 0.022 (2) |
| O34 | 0.3141 (3) | −0.5071 (14) | −0.4091 (16) | 0.0153 (18) |
| O35 | 0.2463 (3) | −0.3006 (14) | −0.2943 (17) | 0.019 (2) |
| O36 | 0.4982 (3) | 0.2185 (13) | −0.0190 (14) | 0.0095 (16) |

parameters (*i.e.* in lower symmetries) was considered unlikely.

Using this neutron-diffraction-refined *C2/m* model as a starting point for further single-crystal refinement, the symmetry was lowered to each of the three maximal non-isomorphic subgroups $C\bar{1}$, *C2* and *Cm*. However, the refinement statistics improved only slightly, to *R* = 0.178, 0.175 and 0.147, respectively. These improvements were considered insufficient to justify the increased number of refined variables. It was necessary to lower

Table 5. *Bond lengths (Å) for the refined single-crystal X-ray structure of $Bi_7Ta_3O_{18}$*

| | | | |
|---|---|---|---|
| Bi1—O17[i] | 2.249 (11) | Bi1—O34[ii] | 2.317 (11) |
| Bi1—O15 | 2.413 (8) | Bi2—O19 | 2.225 (9) |
| Bi2—O4[iii] | 2.234 (11) | Bi2—O2 | 2.268 (11) |
| Bi2—O34 | 2.359 (10) | Bi3—O32 | 2.198 (12) |
| Bi3—O31 | 2.213 (11) | Bi3—O17 | 2.254 (9) |
| Ta4—O7 | 1.927 (10) | Ta4—O14[iv] | 1.966 (10) |
| Ta4—O4 | 1.978 (10) | Ta4—O1 | 1.987 (9) |
| Ta4—O36 | 2.001 (10) | Ta4—O29 | 2.069 (10) |
| Bi5—O5 | 2.247 (8) | Bi5—O16[iv] | 2.306 (10) |
| Bi5—O6 | 2.322 (9) | Bi5—O25[ii] | 2.424 (11) |
| Ta6—O8 | 1.881 (11) | Ta6—O14 | 1.946 (10) |
| Ta6—O10 | 1.962 (10) | Ta6—O1 | 2.008 (9) |
| Ta6—O2 | 2.019 (10) | Ta6—O9 | 2.111 (9) |
| Bi7—O16 | 2.162 (9) | Bi7—O22 | 2.174 (11) |
| Bi7—O20[iii] | 2.192 (10) | Ta8—O28 | 1.965 (9) |
| Ta8—O35 | 1.969 (11) | Ta8—O22 | 1.981 (11) |
| Ta8—O11 | 1.996 (10) | Ta8—O13 | 2.000 (10) |
| Ta8—O32 | 2.006 (11) | Bi9—O27 | 2.268 (9) |
| Bi9—O3 | 2.282 (9) | Bi9—O16 | 2.292 (10) |
| Bi9—O25[i] | 2.319 (11) | Bi10—O12[v] | 2.303 (10) |
| Bi10—O9 | 2.314 (9) | Bi10—O2 | 2.414 (9) |
| Bi11—O12[v] | 2.075 (9) | Bi11—O7[v] | 2.273 (11) |
| Bi11—O8[v] | 2.341 (11) | Bi11—O29 | 2.456 (10) |
| Ta12—O36[vi] | 1.873 (10) | Ta12—O18 | 1.947 (10) |
| Ta12—O30 | 1.893 (11) | Ta12—O3 | 2.092 (9) |
| Ta12—O23 | 1.986 (9) | Bi13—O13[v] | 2.166 (10) |
| Ta12—O27 | 2.108 (10) | Bi13—O24[v] | 2.259 (10) |
| Bi13—O15[v] | 2.247 (9) | Bi14—O21 | 2.018 (9) |
| Bi13—O17 | 2.409 (10) | Bi14—O27[v] | 2.247 (10) |
| Bi14—O6[v] | 2.243 (10) | Ta15—O20 | 1.962 (10) |
| Ta15—O33 | 1.885 (12) | Ta15—O28[iv] | 2.015 (9) |
| Ta15—O11 | 1.975 (10) | Ta15—O15 | 2.092 (9) |
| Ta15—O31 | 2.020 (10) | Bi16—O35[i] | 2.193 (11) |
| Bi16—O34[i] | 2.169 (10) | Bi17—O25[i] | 2.064 (10) |
| Bi16—O33[vii] | 2.277 (12) | Bi17—O30[i] | 2.273 (11) |
| Bi17—O26[vii] | 2.249 (10) | Ta18—O26 | 1.900 (10) |
| Ta18—O10[viii] | 1.899 (10) | Ta18—O18 | 1.985 (10) |
| Ta18—O23[iv] | 1.984 (9) | Ta18—O6 | 2.110 (9) |
| Ta18—O5 | 2.077 (9) | Bi19—O3 | 2.302 (10) |
| Bi19—O24 | 2.218 (10) | Bi19—O21 | 2.372 (9) |
| Bi19—O5 | 2.313 (9) | Bi20—O29[vii] | 2.141 (10) |
| Bi20—O19 | 2.078 (9) | Bi20—O9[i] | 2.220 (10) |

Symmetry codes: (i) $x, y, 1 + z$; (ii) $x, 1 + y, 1 + z$; (iii) $x, y - 1, z$; (iv) $x, 1 + y, z$; (v) $x, y, z - 1$; (vi) $x - \frac{1}{2}, y - \frac{1}{2}, z$; (vii) $x, y - 1, 1 + z$; (viii) $x - \frac{1}{2}, \frac{1}{2} + y, z$.

the symmetry to $C1$ before the refinement statistics improved dramatically, to $R = 0.047$, and the extraneous O-atom peaks in the difference Fourier map disappeared (equivalent positions: $x, y, z; \frac{1}{2} + x, \frac{1}{2} + y, z$). The origin in $C1$ was chosen such that the weighted average of the $C1$ sites Ta8 and Ta15 lies on the pseudo-$C2/m$ $\bar{1}$ site. See §4 for further discussion of the use of the non-standard space group $C1$.

The refinement was further improved ($R = 0.045$) by modelling the ~5% twin component observed during data collection as a mirror-related twin perpendicular to **b**. The volume of this twin component refined to 5.81 (16)% of the total volume. Comparative refinement statistics for the various stages of the refinement described above are given in Table 3. Refinement of

anisotropic displacement parameters for the metal-atom sites gave $R = 0.039$.

The final ($C1$) refined model gave a slightly improved fit when tested against the powder neutron data ($R_p = 0.0426$, $R_{wp} = 0.0321$, $\chi^2 = 25.66$ *versus* $R_p = 0.0455$, $R_{wp} = 0.0342$, $\chi^2 = 29.23$). However, the large number of atomic variables involved in the $C1$ model (including 165 displacive parameters) made refinement impractical.

## 4. Results

Final refined values for the fractional coordinates and $U_{eq}$ values of $Bi_7Ta_3O_{18}$ are given in Table 4 for the single-crystal X-ray ($C1$) refinement. The $C1$ setting is used in order to emphasize the relationship with the $C2/m$ parent structure; it may be transformed to the standard reduced $P1$ setting *via* the real-space transform $\mathbf{a}' = \mathbf{c}$, $\mathbf{b}' = \mathbf{b}$, $\mathbf{c}' = -\frac{1}{2}\mathbf{a} - \frac{1}{2}\mathbf{b} - \mathbf{c}$. Bond lengths for the refined $C1$ structure are given in Table 5. The final observed, calculated and difference powder neutron diffraction profiles for the Rietveld refinement in $C2/m$ are shown in Fig. 1.†

## 5. Discussion

The final refined model ($C1$) from the single-crystal X-ray data is shown in Figs. 2(a) and (b). The $C2/m$ structure derived from the X-ray and neutron diffraction data is topologically equivalent to this $C1$ model, with atom positions differing by less than 0.25 Å. The structure is essentially 'layered' perpendicular to the long ($a$) axis, as can be seen in these projections. The Ta atoms are coordinated in regular $TaO_6$ octahedra, which form columns along the [010] direction (Fig. 2b). Octahedra within these columns are rotated through ~10° about the [001] direction (Fig. 2b). The coordination environments of the Bi atoms appear to be related to the cubic (eightfold) coordination found in fluorite, distorted by the presence of $TaO_6$ octahedra such that the Bi—O bond lengths vary between 2.0 and 3.0 Å. Setting the maximum Bi—O bond length at 2.75 Å allows three distinct classes of site to be identified: (i) Bi2, Bi3, Bi7, Bi13, Bi16 and Bi19 have distorted octahedral coordination; (ii) Bi11, Bi14, Bi17 and Bi20 are located on the basal planes of square (Bi11, Bi14) or pentagonal (Bi17, Bi20) pyramids; (iii) Bi1, Bi5, Bi9 and Bi10 are offset from the centre of trigonal prisms. Examples of each of these coordination polyhedra are shown in Fig. 3.

Pyramidal and trigonal prismatic coordination environments are typically observed around cations with stereochemically active electron lone pairs, such as $Bi^{3+}$. The archetypes are $\alpha$-PbO and $SbCl_3$ (or $XeO_3$), respectively (Hyde & Andersson, 1989). The distorted
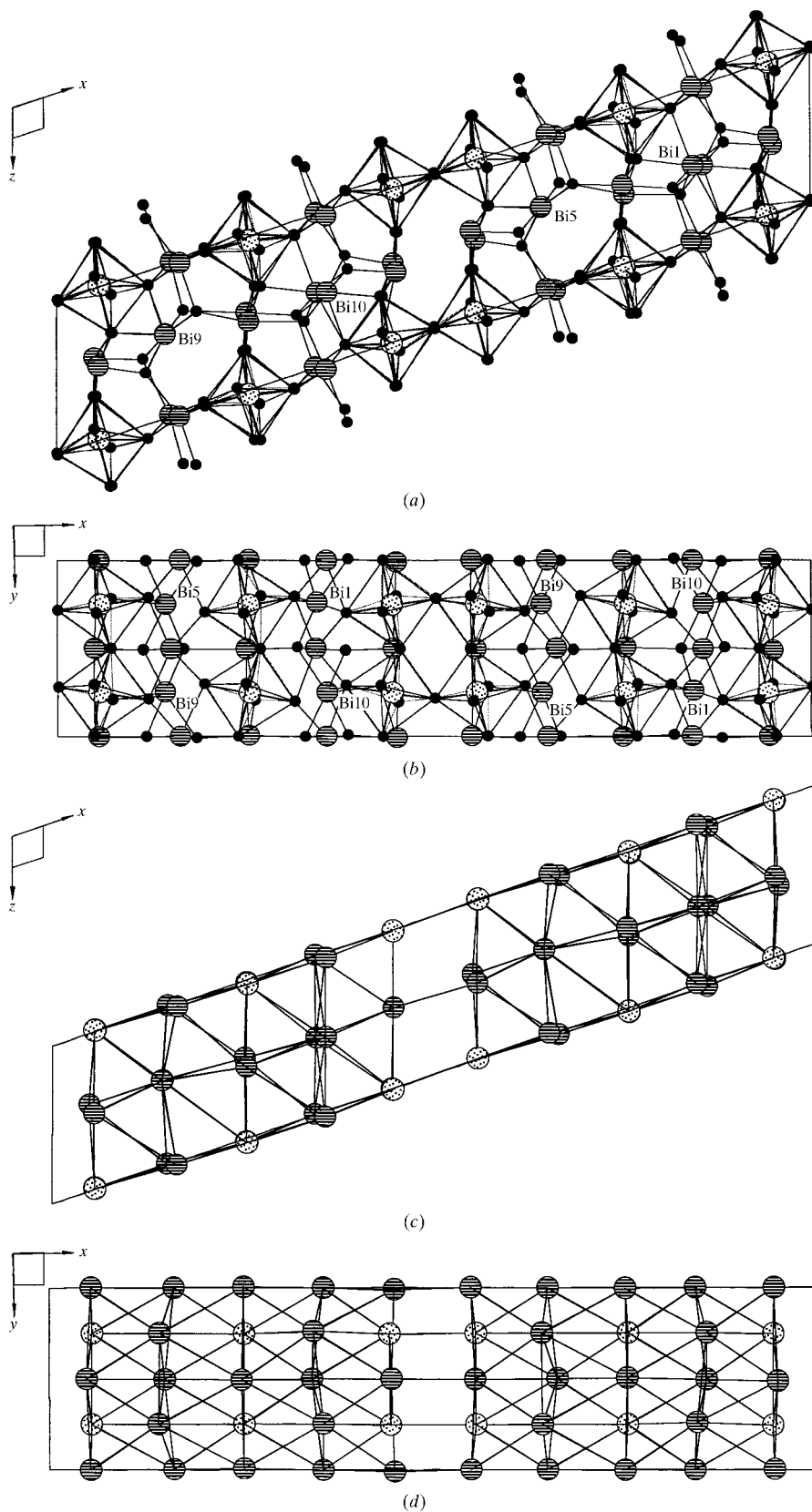
(a)

(b)

(c)

(d)

Fig. 2. The final refined (C1) structure of Bi$_7$Ta$_3$O$_{18}$ viewed down (a) the [010] axis and (b) the [001] axis. (c) and (d) show only metal atoms and their nearest-neighbour connectivity, highlighting the stacking faults in the f.c.c. array. Bi atoms are striped, Ta atoms are dotted and O atoms are black.

Table 6. *Bond-valence sums (Brese & O'Keeffe, 1991) for the single-crystal X-ray and Rietveld-refined structures of* $Bi_7Ta_3O_{18}$

| Atom | $C2/m$ | $C1$ | Atom | $C2/m$ | $C1$ |
|------|--------|------|------|--------|------|
| Bi1  | 2.688  | 2.655 | Bi2  | 3.290 | 3.101 |
| Bi3  | 2.958  | 3.069 | Ta4  | 4.996 | 5.025 |
| Bi5  | 2.688  | 2.741 | Ta6  | 4.996 | 5.064 |
| Bi7  | 2.958  | 3.241 | Ta8  | 5.041 | 5.003 |
| Bi9  | 2.688  | 2.839 | Bi10 | 2.688 | 2.699 |
| Bi11 | 3.229  | 3.103 | Ta12 | 4.996 | 5.177 |
| Bi13 | 3.109  | 3.133 | Bi14 | 2.941 | 3.218 |
| Ta15 | 5.041  | 5.002 | Bi16 | 3.109 | 3.111 |
| Bi17 | 3.229  | 3.147 | Ta18 | 4.996 | 5.044 |
| Bi19 | 3.290  | 3.042 | Bi20 | 2.941 | 3.197 |
| O1   | 1.788  | 1.945 | O2   | 2.011 | 2.055 |
| O3   | 2.011  | 2.064 | O4   | 2.011 | 2.032 |
| O5   | 2.011  | 2.108 | O6   | 1.999 | 2.111 |
| O7   | 1.946  | 1.832 | O8   | 1.946 | 1.803 |
| O9   | 1.999  | 2.120 | O10  | 2.036 | 2.011 |
| O11  | 2.072  | 1.936 | O12  | 2.358 | 2.300 |
| O13  | 1.876  | 2.009 | O14  | 2.022 | 1.939 |
| O15  | 1.876  | 1.941 | O16  | 2.136 | 2.179 |
| O17  | 2.136  | 2.065 | O18  | 2.022 | 1.940 |
| O19  | 1.926  | 2.177 | O20  | 1.973 | 1.963 |
| O21  | 1.926  | 2.121 | O22  | 1.973 | 1.964 |
| O23  | 1.788  | 1.920 | O24  | 1.988 | 1.968 |
| O25  | 2.358  | 2.255 | O26  | 1.946 | 1.959 |
| O27  | 1.999  | 2.147 | O28  | 2.072 | 1.945 |
| O29  | 1.999  | 2.045 | O30  | 1.946 | 1.922 |
| O31  | 1.973  | 1.956 | O32  | 1.973 | 1.907 |
| O33  | 1.876  | 1.911 | O34  | 1.988 | 2.167 |
| O35  | 1.876  | 1.899 | O36  | 2.036 | 2.000 |

octahedral sites also reflect the stereochemical influence of the lone pair.

Bond-valence sums (Brese & O'Keeffe, 1991) are given in Table 6 for both the $C2/m$ and $C1$ refined models. The results are of a similar standard in both space groups, and do not immediately indicate the driving force behind the symmetry lowering. It is significant, however, that for both models the Bi atoms in trigonal prismatic sites have bond-valence sums furthest from the expected value of 3.0. In $C2/m$, these four atoms are equivalent. Fig. 2(b) shows that in $C1$, Bi1 and Bi10 have broken the mirror plane perpendicular to **b**, and Fig. 2(a) shows that the twofold rotation axis about **b** now no longer maps the Bi1/Bi10 pair onto the Bi5/Bi9 pair. This is by far the most significant

deviation from $C2/m$ symmetry in the final refined $C1$ structure. The subsequent improvement in bond-valence sums is small and the breaking of symmetry may be more an indication of the instability of the coordination environment than the inherent stability of the lower-symmetry configuration. Note that the mirror twin modelled in the refinement is accomplished by simply exchanging the $x$ coordinates of Bi1 and Bi10, whereas a twin against the twofold axis would involve a split of the Bi5/Bi9 pair rather than the Bi1/Bi10 pair. That the structure is closer to $Cm$ than to $C2$ is also supported by the comparative refinement statistics presented in Table 3.

No other reasons for symmetry lowering could be found; there is no evidence of unfavourably short metal–oxygen or oxygen–oxygen contacts in the higher symmetry, nor does the regularity of the $TaO_6$ octahedra, in terms of either O—Ta—O angles or Ta—O distances, appear to be compromised.

Although there is no unambiguous fluorite-type subcell in the diffraction patterns of $Bi_7Ta_3O_{18}$, a number of fluorite-like patterns were obtained by electron diffraction (Ling *et al.*, 1998). The origin of these patterns can be seen in the real-space structure. Figs. 2(c) and (d) are equivalent to Figs. 2(a) and (b), respectively, but show only the metal-atom array and its nearest-neighbour connectivity. The continuous blocks have an f.c.c. (*i.e.* fluorite) arrangement. Fluorite units therefore exist continuously throughout the structure, except at the $x = 0$ and $x = \frac{1}{2}$ planes (perpendicular to the $[111]_{\text{fluorite}}$ direction). Fluorite-type blocks are 'stepped' on these planes, two adjacent metal layers forming a primitive hexagonal, rather than an f.c.c., array. These stacking faults make it meaningless (and effectively impossible) to relate a unique, average fluorite-type subcell to the unit cell of $Bi_7Ta_3O_{18}$ in diffraction space, despite a strong and obvious relationship to a fluorite substructure in real space.

Despite the relationship to fluorite in the metal-atom array of $Bi_7Ta_3O_{18}$, the projections shown in Fig. 2 are clearly the most important in terms of gaining an understanding of the real structure. That these projections bear no strong relationship to any fluorite-like projections is a practical indication that $Bi_7Ta_3O_{18}$
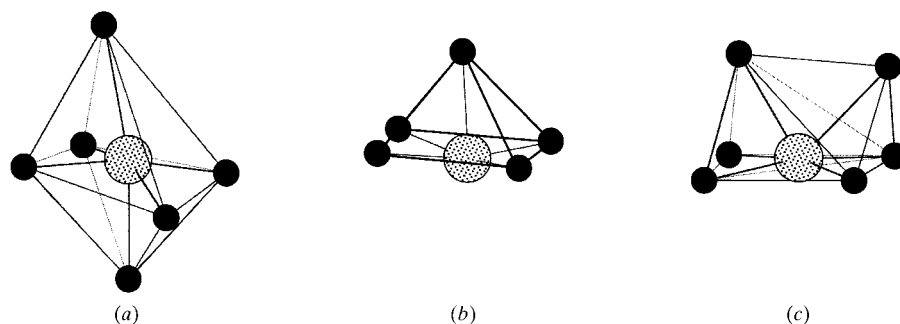


(a)  (b)  (c)

Fig. 3. The coordination environments of (a) Bi2, (b) Bi17 and (c) Bi1.

should not be considered as a modulated $\delta$-$Bi_2O_3$-related phase, but as a distinct structure type.

## References

Allnat, A. R. & Jacobs, P. W. M. (1961). *Proc. R. Soc. London Ser. A*, **260**, 350–369.

Allnat, A. R. & Jacobs, P. W. M. (1967). *Chem. Rev.* **67**, 681–705.

Brese, N. E. & O'Keeffe, M. (1991). *Acta Cryst.* B**47**, 192–197.

Gattow, G. & Schröder, H. (1962). *Z. Anorg. Allg. Chem.* **318**, 176–189.

Hall, S. R., Flack, H. D. & Stewart, J. M. (1992). Editors. *Xtal*3.2 *Reference Manual.* Universities of Western Australia, Australia, Geneva, Switzerland, and Maryland, USA.

Harwig, H. A. (1978). *Z. Anorg. Allg. Chem.* **444**, 151–166.

Hull, S., Smith, R. I., David, W. I. F., Hannon, A. C., Mayers, J. & Cywinski, R. (1992). *Physics*, B**180&181**, 1000–1002.

Hyde, B. G. & Andersson, S. (1989). *Inorganic Crystal Structures*, pp. 257–271. New York: Wiley.

Larson, A. C. & Von Dreele, R. B. (1991). *GSAS. The General Structure Analysis System.* Los Alamos National Laboratory, Los Alamos, USA.

Levin, E. M. & Roth, R. S. (1964). *J. Res. Natl Bur. Stand. Sect. A*, **68**, 197–206.

Ling, C. D., Withers, R. L., Schmid, S. & Thompson, J. G. (1998). *J. Solid State Chem.* **137**, 42–61.

Sleight, A. W. (1980). *Science*, **208**, 895–900.

Takahashi, T. & Iwahara, H. (1978). *Mater. Res. Bull.* **13**, 1447–1453.

Von Dreele, R. B. (1990). Unpublished work.

Zachariasen, W. H. (1968). *Acta Cryst.* A**24**, 212–216.

Zhou, W. (1992). *J. Solid State Chem.* **101**, 1–17.